05

Pd−Fe alloy film with high magnetic gradient: structural and magnetic properties

© I.V. Yanilkin,[1,2] A.I. Gumarov,[1,2] I.A. Golovchanskiy,[3,4,5] G.F. Gizzatullina,[1] A.G. Kiiamov,[1] B.F. Gabbasov,[1] R.V. Yusupov,[1] L.R. Tagirov[1,2]

[1] Kazan Federal University,
420008 Kazan, Russia
[2] Zavoisky Physical-Technical Institute, FRC „Kazan Scientific Center of RAS"
420029 Kazan, Russia
[3] National University of Science and Technology MISIS,
119049 Moscow, Russia
[4] Moscow Institute of Physics and Technology, National Research University,
141700 Dolgoprudny, Moscow Region, Russia
[5] Dukhov Research Institute of Automatics (VNIIA),
127055 Moscow, Russia
e-mail: yanilkin-igor@yandex.ru

Received September 1, 2022
Revised October 20, 2022
Accepted October 20, 2022

An epitaxial film of the Pd−Fe alloy 116 nm thick with an iron concentration varying in depth from 2 at.% to 50 at.% has been synthesized. An experimental depth distribution profile of iron was obtained as a result of stepwise etching of the film surface with Ar^+ ions. Profiling has shown that, as a result of annealing, the impurity was redistributed in the film, and a layer of the $L1_0$-phase with a constant concentration was formed near the film surface. After removal of the $L1_0$-phase, the film exhibits „easy-plane"anisotropy. The study of spin-wave resonance spectra showed the presence of several modes of standing spin waves, the number of which depends on the residual film thickness.

Keywords: graded magnetic materials, molecular beam epitaxy, palladium-iron alloys, X-ray diffraction, spin-wave resonance.

DOI: 10.21883/TP.2023.02.55473.213-22

Introduction

In the last few years, in scientific literature related to the study of magnetic materials and alloys, one can meet the term „Graded Magnetic Materials" (GMM), these are materials that exhibit spatially dependent magnetic properties (see, for example, an review [1] and references therein, and a paper [2]). GMMs attract the attention of researchers from both fundamental and applied points of view, because by selecting profiles of composition distribution through depth it becomes possible to control the exchange interaction and the corresponding effective or local Curie temperatures on scales of several nanometers [1,3,4]. One of the interesting directions in the study of magnetic materials with spatially modulated magnetic properties is the study of thin ferromagnetic films, in which the excitation and propagation of spin waves (magnons), which are of interest today for practical applications in magnon spintronics, are observed [5–7]. In this respect, palladium-iron alloys are promising model materials and have a number of unique properties, which include high stability and the ability to fine-tune the magnetic parameters via concentration change of iron admixture [8], as well as full mutual solubility of iron and palladium with the formation of a continuous series of solid solutions of the austenitic class [9,10]. At the same time, there is already a proven technology for the films synthesis of alloy $Pd_{1-x}Fe_x$ ($x = 0.01-0.1$) with high crystallinity and low roughness [11]. Such alloys can become a powerful tool for creating a spatially magnetic heterogeneity of any geometry, which, in its turn, makes it possible to control the spin wave dispersion law. For example, an epitaxial film of the Pd−Fe alloy 116 nm thick with linear change in the magnetic impurity concentration from 3 to 10 at.% [7] was recently studied, in which an anomalous spin-wave resonance was observed [12]. It is known that in the Pd−Fe alloy with the iron concentration increasing to values exceeding 10 at.% the magnetic properties change non-linearly [13–15]. In this regard, the study of the Pd−Fe alloy film, in which the magnetic characteristics change significantly with depth, seems to be an interesting and intriguing problem, the solution of which will make it possible to establish the operating range of iron concentrations at which the spin-wave resonance will manifest itself in a classical way, i.e. the number of modes will increase with increasing of film thickness and gradient of magnetic properties. In the present paper, we synthesized the epitaxial film of the Pd−Fe alloy 116 nm thick, in which the iron content varies linearly from 2 to 50 at.%

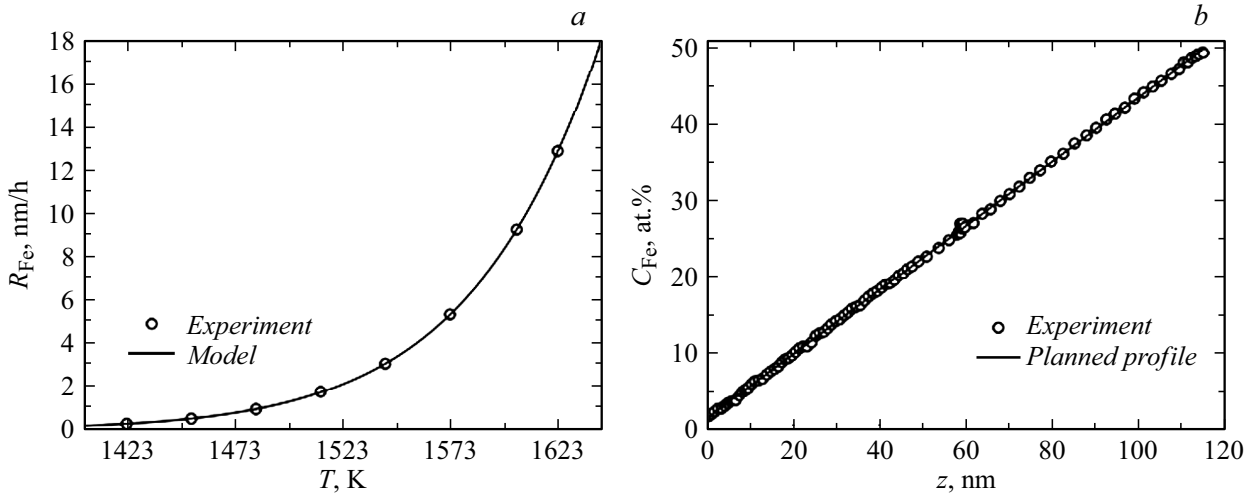

Figure 1. Rate of deposition of iron from effusion cell vs. its temperature (a) and the experimental iron concentration profile obtained from the calibration of the rate of deposition during spattering on a quartz thickness sensor (b).

through thickness, and studied its structural and magnetic properties.

1. Experimental part

To obtain the Pd–Fe alloy film, high-purity (99.95%) Pd and Fe metals were evaporated from Knudsen effusion cells in the form of molecular beams and deposited on a rotating substrate. The dependence of the material deposition rate on the cell temperature was established experimentally using a quartz thickness sensor with a measurement accuracy of 0.01 nm. The obtained dependence of the deposition rate on temperature can be well described in the approximation of ideal gas kinetic theory and using the Clapeyron–Clausius equation for the sublimation process, which gives $\nu \sim \exp\left(-\frac{B}{kT}\right)\left(\sqrt{T}\right)^{-1}$ (Fig. 1, a). Thus, knowing the cell temperature it is possible to predict with good accuracy the rate of material delivery on the substrate. Varying the cell temperature, and thereby changing the deposition rate, it is possible to obtain alloy films with any desired profile of composition distribution through thickness. Below there is an example for a calibration sample of the Pd–Fe alloy with a near-linear iron concentration distribution profile $C_{Fe}(z)$ deposited on the quartz thickness sensor (Fig. 1, b). Here and below, z is the distance from the substrate surface. To obtain a heterogeneous distribution of the iron impurity in the palladium matrix, we divided the deposition process into 10 steps, at each of which the cell temperature change rate was set, while the entire sequence of cell temperature change was uploaded into the Eurotherm 3504 temperature controller. Subsequently, the epitaxial film of the Pd–Fe alloy on a MgO substrate was grown in similar way (for a detailed description of the experiment, see below).

To provide the required concentration distribution of the elements through the film thickness, the temperature of the palladium cell was fixed at 1594 K, and of the iron cell — changed in the range of 1323–1619 K. Since the goal was to obtain a smooth epitaxial film, the deposition took place in several stages. First, a 5 nm thick Pd–Fe layer was deposited onto a (001)-oriented substrate of single-crystal MgO heated to $T = 673$ K. Then the substrate heating was stopped, and further film deposition was carried out on the cooling substrate. The total deposition time was 358 min and was chosen so as to finally obtain the film with thickness $d = 116$ nm. The final stage of the synthesis was the film annealing at a temperature of 873 K for 2 h. The entire synthesis process was carried out under ultrahigh vacuum conditions ($5 \cdot 10^{-10}$ mbar) in a molecular beam epitaxy chamber manufactured by SPECS (Germany). The structural perfection of the film was monitored *in situ* after its synthesis using low-energy electron diffraction (LEED) and *ex situ* X-ray diffraction analysis (XDA) at room temperature using Bruker D8 ADVANCE X-ray diffractometer in Bragg–Brentano geometry. Elemental analysis was carried out by X-ray photoelectron spectroscopy (XPS from SPECS) using the depth profiling method by etching the film with Ar^+ ions. The ion energy was 2 keV, and the current density — 10 μA/cm^2. The profiling process was divided into 4 stages. At each stage, several cycles of etching and XPS analysis were performed, after which the sample was removed from the analytical vacuum chamber, and its structural and magnetic properties were studied. The magnetic characteristics of the film were studied by vibrating magnetometry with Quantum Design PPMS-9 system and by spin-wave resonance (SWR) with Bruker ESP300 continuous microwave X-band spectrometer in a wide range of fields 0–1.4 T and temperature range of 20–300 K.

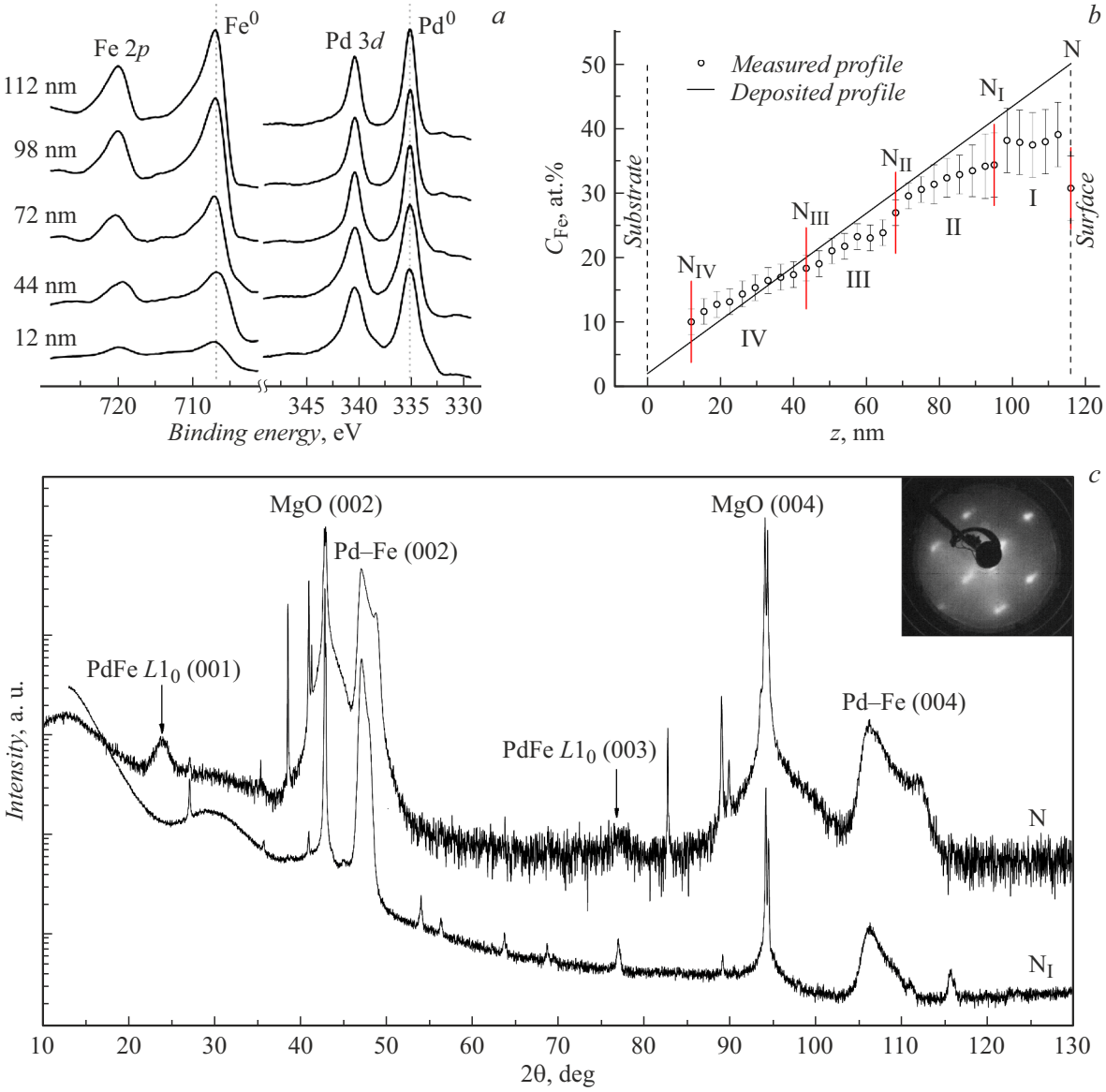

Figure 2. *a* — XPS spectra of Fe2*p*- and Pd3*d*-electrons for various residual film thicknesses; *b* – profiles of iron concentration distribution in the Pd−Fe film, specified during deposition (line) and measured by XPS (circles), etching stages are indicated by four segments; *c* — X-ray diffraction patterns of the original film and same film after the first stage of etching. In the insert — the LEED pattern (152 eV) obtained from the surface of the Pd−Fe film just after synthesis.

2. Results and discussion thereof

XPS study of the film using layer-by-layer etching (Fig. 2, *a*) showed a significant change in the Pd/Fe ratio through the thickness. Fig. 2, *b* shows the profiles of the iron concentration distribution through the depth of the film specified during deposition and measured, divided into four segments corresponding to the stages of etching the film surface with Ar^+ ions, which are indicated by Roman numerals I, II, III, IV. Here and below, the initial sample is denoted by the letter N. The same sample after the first etching stage is designated as N_I, after the second etching stage as N_{II}, etc. (see Fig. 2, *b* and the summary Table). The general nature of the measured profile generally corresponds to the set one, however, there are two features. First, a region $\sim 15-20$ nm thick near the film surface is determined, which is characterized by a constant iron concentration. It was established by X-ray diffraction analysis that this „plateau“ corresponds to the Pd−Fe phase with an atomically ordered structure of $L1_0$ type. Since the profile with a constant iron concentration gradient was initially specified, the „plateau“region was probably formed as a result of thermal annealing at the last stage of film synthesis, during which the iron impurity was redistributed. and a stable $L1_0$ phase was formed. The value of the iron concentration in the $L1_0$-phase layer 38−40 at.%

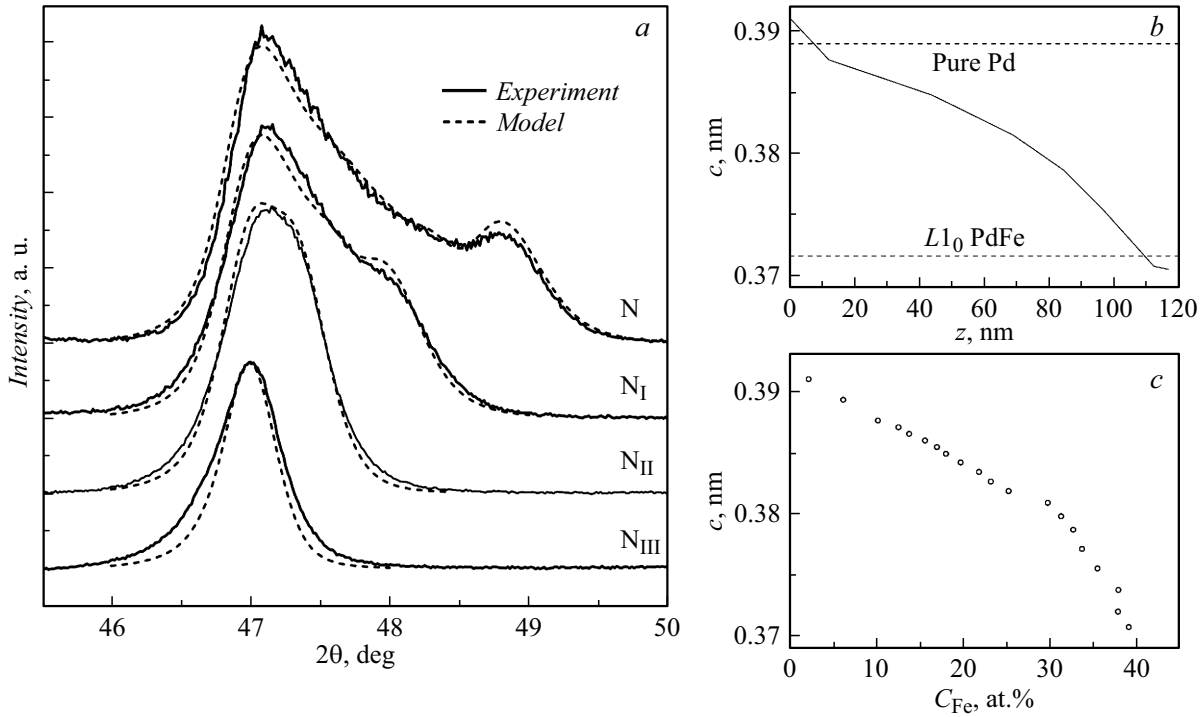

Figure 3. *a* — the shape of diffraction (002)-maximum for the initial sample and after I, II, and III stages of etching; the solid line shows the measured X-ray diffraction patterns, and the dashed lines — calculated; *b* — calculated dependence of lattice parameter c on the distance to the film surface z; *c* — experimental dependence of lattice parameter c on iron concentration C_{Fe}.

The nomenclature of the samples and the parameters of the PdFe film — initial and after each stage of etching with Ar^+ ions: thickness (d), saturation magnetic moment (M_s), coercive field (H_c), as well as the number of resonant modes (measured and calculated)

Stage of etching	Sample	d, nm	M_s, * nA·m^2	$\mu_0 H_c$, mT	Number of modes	
					Experiment	Calciulation
–	N	116	344	9.5	2	9
I	N_I	98	267	9.3	3	7
II	N_{II}	68	167	0.9	3	4
III	N_{III}	44	98	2	2	2
IV	N_{IV}	12	45	2	1	1

Note. * — Temperature $T = 20$ K.

was determined with a significant error associated with the features of the concentration determination in the XPS method, which systematically underestimates the iron concentration in the $Pd_{1-x}Fe_x$ with $x \sim 50$ at.%. Second, in the region of the interface with the substrate, the iron concentration exceeds the specified value. We attribute this to heterogeneous etching, which leaves areas with a thicker film in the later stages of etching.

Point reflections appear in the LEED pattern of the initial film (Fig. 2, *c*, insert), indicating the single-crystal nature of the film obtained after annealing. Also, in the X-ray diffraction pattern of the original film (Fig. 2, *c*), during θ angle scanning peaks (001), (002), (003) and (004) were identified. At the same time, φ scanning was performed for (202) reflex (not shown here), for which its φ direction matching in the film and substrate was found. All this indicates that the synthesized film is epitaxial through its full thickness.

The presence of (001) and (003) peaks indicates the tetragonal $L1_0$-phase presence in the film. The low intensity and large width of the (001)-reflex indicates a small thickness of the layer containing this phase, for which the diffraction calculation gives the thickness estimate of $\sim 5-10$ nm. After the first etching (Fig. 2, *c*) (001) and (003) reflexes completely disappear, which also indicates a small thickness of the $L1_0$-phase layer and its localization near the surface.

Peaks (002) and (004) appear after all etching stages, but their shape changes significantly (Fig. 3, *a*). From the nature of the reflex profile change, the distribution of the lattice parameter $c(z)$ through the film thickness was determined (Fig. 3, *b*). For this, diffraction by a one-dimensional structure with a parameter distributed through depth was calculated (Fig. 3, *a*, dashed line). As a result of comparison of the obtained dependences of the lattice parameter $c(z)$ and the iron concentration $C_{Fe}(z)$ on the location in the Pd–Fe film, it was found how these values in the synthesized film correlate to each other (Fig. 3, *c*). It is worth noting that the range of c values (shown by dashed lines in Fig. 3, *b*) corresponds well to the lattice parameters for pure palladium and the $L1_0$ phase $Pd_{50}Fe_{50}$.

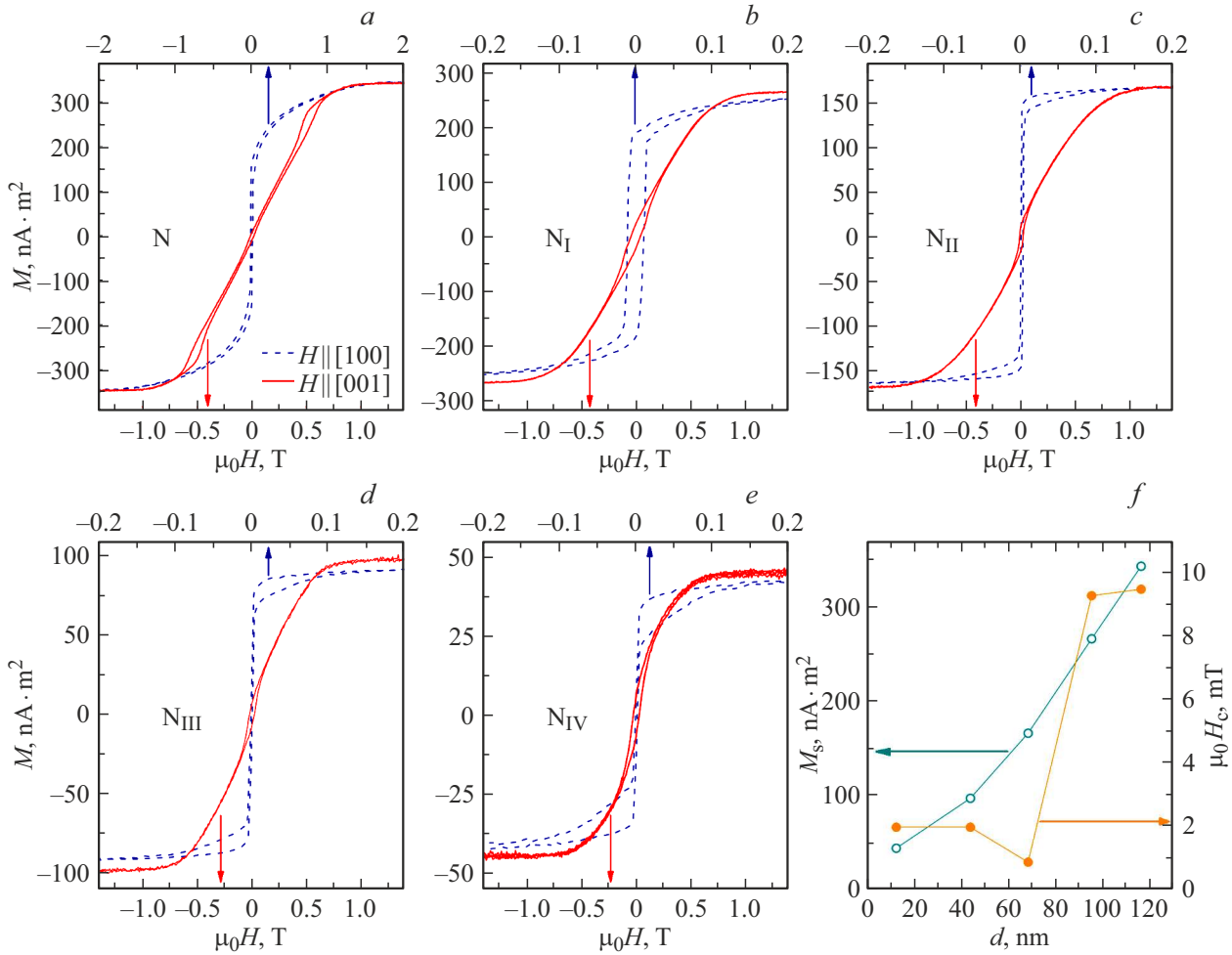

Figure 4. Magnetic hysteresis loops for the initial film (a) and after I–IV etching steps (b–e respectively), measured at a temperature of 20 K for different directions of the external magnetic field; f — values of the magnetic moment of the sample and the coercive field for **H** || [100] after each etching step.

A slight excess of this range (going beyond the dashed lines in Fig. 3, b) can also be explained. For example, for the $L1_0$-phase of $Pd_{50}Fe_{50}$ the lattice parameter c less than 0.37 nm was observed in [16] for thin epitaxial films up to 10 nm thick.

Fig. 4, a–e shows the magnetic hysteresis loops for two different directions of the magnetic field obtained after each etching stage. In all cases, almost complete coincidence of the shape of the loops is observed for the field direction **H** || [100] and **H** || [110] in the film plane, which is unusual for the ferromagnetic cubic system Pd–Fe with low (less than 10 at.%) iron content [8]. In the original film, the presence of the $L1_0$-phase manifests itself in the observation of hysteresis in the region of fields ±0.5 T at **H** || [001] (field along the normal to the film), and also in large saturation fields (~ 2 T) at **H** || [100] (Fig. 4, a). It can be seen from the shape of the switching curve at **H** || [001] that the domain structure formation begins in sufficiently high fields, which is typical for thick continuous films of the Pd–Fe $L1_0$-phase [17]. We believe that for our film the effective thickness of the $L1_0$-phase layer is increased due to the underlying layers. A similar effect was observed in the paper [18], where PtFe epitaxial layers were combined with $A1$ and $L1_0$ structures.

The heterogeneous magnetization of the film leads to a nonlinear change in its magnetic moment depending on the residual thickness of the film (Fig. 4, f). When a magnetic field is applied in the plane of the film, a jump in the magnitude of the coercive field H_c from ~ 9.5 to ~ 1 mT was found at film thickness of about 85 nm (Fig. 4, f), which corresponds to the iron concentration ~ 30 at.% (Fig. 2, a). These values qualitatively correlate with the values H_c over 30 mT for $x > 30$ at.% and below 2.5 mT for $x < 10$ at.% for homogeneous epitaxial films $Pd_{1-x}Fe_x$ [8,19].

The study of the magnetic resonance spectra of the Pd–Fe film showed the presence of several modes of standing spin waves (SSWs) (Fig. 5, a), the number of which depended on the residual film thickness after each etching stage (Fig. 5, b). In this case, an anomaly

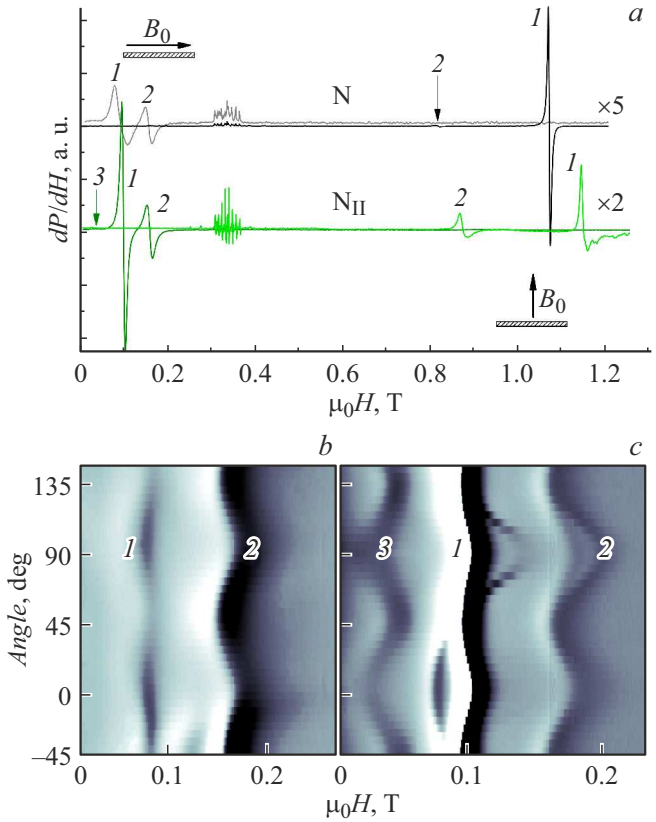

Figure 5. Magnetic resonance spectra for parallel and perpendicular field orientations B_0 with respect to the film plane (a). The upper pair of spectra — for the initial film, the lower one — after the second etching stage. Orientation dependences of resonance fields (field B_0 in the plane) measured for the initial sample (b) and after the second etching stage (c). In the Figures, the serial number of the modes is indicated by digits.

appears: the number of modes does not increase with film thickness increasing, but, on the contrary, decreases. To estimate the scale of the anomaly we calculated the number of modes according to the theory of standing spin waves [12] in the approximation of magnetization linearly varying through thickness, using the parameters obtained for heterogeneous Pd–Fe film in [7] (see Table). As can be seen, at thickness ~ 50 nm corresponding to the iron concentration ~ 20 at.% there is a difference between the results of calculation and experiment, which grows with thickness increasing. The reason for this difference, in our opinion, is the nonlinear nature of the change in magnetocrystalline anisotropy in $Pd_{1-x}Fe_x$ crystals, up to a change in the sign of the anisotropy constant K_1 at $x \sim 18$ at.% and the transition from cubic to uniaxial symmetry at $x \sim 37$ at.% [13–15]. The change in the sign of cubic anisotropy in our case manifested itself in the angular dependences of the resonance field. As can be seen from Fig. 5, *c*, modes *1* and *2* are in antiphase with mode *3*. It can be said that the main absorption of microwave radiation occurs in different regions of the film thickness. Modes *1* and *2* reflect absorption in the region of low iron concentrations $x < 18$ at.% ($K_1 < 0$), while the mode *3* — for $x > 18$ at.% ($K_1 > 0$). The presence of film regions with anisotropy constants differing in sign is most likely the reason why the shape of the hysteresis loops does not depend on the direction of the field in the plane (Fig. 4), as was mentioned above.

On the basis of the SWR data obtained, it can be said that the presence of a radically changing anisotropy through the film thickness suppresses the excitation of standing spin waves in it. Besides, it is much more difficult to analyze and model such systems. We consider that the concentration range $x < 18$ at.%, in which cubic anisotropy with constant $K_1 < 0$ is observed, is most suitable for engineering the properties of SSW in heterogeneous Pd–Fe films. Note that at $x > 12$ at.% Pd–Fe alloys are already ferromagnetic at room temperature.

Conclusion

The analysis of all obtained experimental data has shown that film of the ferromagnetic alloy Pd–Fe 116 nm thick, and change in the iron concentration in wide range from 2 to 50 at.% exhibits a significant nonlinear change in magnetic properties through the thickness. It was established that, first of all, this is due to the tetragonal $L1_0$-phase formation in the region of high iron concentrations, the magnetic properties of which differ significantly from those of the remaining part, which has cubic symmetry. However, in the region of medium concentrations (2–30 at.%) also, the nonlinearity of the magnetic properties is also observed, which is associated with change in the sign of the anisotropy constant K_1 in the vicinity of the concentration 18 at.%. The significant non-linearity of the anisotropy leads to the suppression of the spin-wave resonance. It was found that the concentration range $x < 18$ at.% is most suitable for engineering the standing spin waves in Pd–Fe gradient films.

Acknowledgments

The authors are grateful to V.S. Stolyarov (MFTI) for useful comments and fruitful discussion of the results obtained in this paper.

Funding

The experimental part of the work was carried out under the Strategic Academic Leadership Program of the Kazan (Volga Region) Federal University (Priority 2030). Theoretical studies were carried out with the support of the Ministry of Science and Higher Education of the Russian Federation (project № 0718-2020-0025).

Conflict of interest

The authors declare that they have no conflict of interest.

References

[1] L. Fallarino, B.J. Kirby, E.E. Fullerton. J. Phys. D: Appl. Phys., **54** (30), 303002 (2021). DOI: 10.1088/1361-6463/abfad3

[2] V.A. Ignatchenko, D.S. Tsikalov. J. Appl. Phys., **127** (12), 123903 (2020). DOI: 10.1063/1.5143499

[3] B.J. Kirby, H.F. Belliveau, D.D. Belyea, P.A. Kienzle, A.J. Grutter, P. Riego, A. Berger, C.W. Miller. Phys. Rev. Lett., **116** (4), 047203 (2016). DOI: 10.1103/PhysRevLett.116.047203

[4] L. Fallarino, E.L. Rojo, M. Quintana, J.S.S. Gallo, B.J. Kirby, A. Berger. Phys. Rev. Lett., **127**, 147201 (2021). DOI: 10.1103/PhysRevLett.127.147201

[5] R.A. Gallardo, P. Alvarado-Seguel, T. Schneider, C. Gonzalez-Fuentes, A. Roldán-Molina, K. Lenz, J. Lindner, P. Landeros. New J. Phys., **21** (3), 033026 (2019). DOI: 10.1088/1367-2630/ab0449

[6] P. Landeros, R.A. Gallardo, G. Carlotti. J. Phys.: Condensed Matter., **33** (41), Ch. 16, 413001 (2021). DOI: 10.1088/1361-648X/abec1a

[7] I.A. Golovchanskiy, I.V. Yanilkin, A.I. Gumarov, B.F. Gabbasov, N.N. Abramov, R.V. Yusupov, R.I. Khaibullin, L.R. Tagirov. Phys. Rev. Mater., **6**, 064406 (2022). DOI: 10.1103/PhysRevMaterials.6.064406

[8] A. Esmaeili, I.V. Yanilkin, A.I. Gumarov, I.R. Vakhitov, B.F. Gabbasov, R.V. Yusupov, D.A. Tatarsky, L.R. Tagirov. Sci. Chin. Mater., **64** (5), 1246 (2021). DOI: 10.1007/s40843-020-1479-0

[9] T.B. Massalski, H. Okamoto, P. Subramanian, L. Kacprzak, W.W. Scott. *Binary Alloy Phase Diagrams* (Metals Park, OH: American Society for Metals, 1986)

[10] E.M. Savitsky, V.P. Polyakova, M.A. Tylkina. *Splavy palladiya* (Nauka, M., 1967) (in Russian)

[11] A. Esmaeili, I.V. Yanilkin, A.I. Gumarov, I.R. Vakhitov, B.F. Gabbasov, A.G. Kiiamov, A.M. Rogov, Yu.N. Osin, A.E. Denisov, R.V. Yusupov, L.R. Tagirov. Thin Solid Films, **669**, 338 (2019). DOI: 10.1016/j.tsf.2018.11.015

[12] T.G. Rappoport, P. Redliński, X. Liu, G. Zaránd, J.K. Furdyna, B. Jankó. Phys. Rev. B, **69** (12), 125213 (2004). DOI: 10.1103/PhysRevB.69.125213

[13] N. Miyata, K. Tomotsune, H. Nakada, M. Hagiwara, H. Kadomatsu, H. Fujiwara. J. Phys. Society Jpn., **55** (3), 946 (1986). DOI: 10.1143/JPSJ.55.946

[14] N. Miyata, M. Hagiwara, H. Kunitomo, S. Ohishi, Y. Ichiyanagi, K. Kuwahara, K. Tsuru, H. Kadomatsu, H. Fujiwara. J. Phys. Society Jpn., **55** (3), 953 (1986). DOI: 10.1143/JPSJ.55.953

[15] N. Miyata, H. Asami, T. Mizushima, K. Sato. J. Phys. Society Jpn., **59** (5), 1817 (1990). DOI: 10.1143/JPSJ.59.1817

[16] M. Futamoto, M. Nakamura, M. Ohtake, N. Inaba, T. Shimotsu. AIP Advances, **6** (8), 085302 (2016). DOI: 10.1063/1.4960554

[17] V. Gehanno, Y. Samson, A. Marty, B. Gilles, A. Chamberod. J. Magn. Magn. Mater., **172** (1–2), 26 (1997). DOI: 10.1016/S0304-8853(97)00089-9

[18] J. Lee, B. Dymerska, J. Fidler, V. Alexandrakis, T. Speliotis, D. Niarchos, P. Pongratz, D. Suess. Phys. Status Solidi A, **210** (7), 1305 (2013). DOI: 10.1002/pssa.201228731

[19] C.F. Wang, K.M. Kuo, C.Y. Lin, G. Chern. Solid State Commun., **149**, 1523 (2009). DOI: 10.1016/j.ssc.2009.06.005